Electronic structure of dilute Ni_xAu_{1-x} alloys

1996 J. Phys.: Condens. Matter 8 5569

(http://iopscience.iop.org/0953-8984/8/30/007)

J. Phys.: Condens. Matter **8** (1996) 5569–5583. Printed in the UK

Electronic structure of dilute Ni_xAu_{1-x} alloys

Ge Meng, R Claessen†, F Reinert, R Zimmermann, P Steiner and S Hüfner
Fachrichtung Experimentalphysik, Universität des Saarlandes, D-66041 Saarbrücken, Germany

Received 19 March 1996

Abstract. The electronic structure of dilute Ni_xAu_{1-x} alloys has been studied by synchrotron-radiation-induced photoemission and bremsstrahlung isochromat spectroscopy. The use of photon energies at the Au 5d Cooper minimum and the Ni 2p–3d absorption threshold strongly enhances the spectral distribution of the Ni 3d impurity states with respect to the Au states. It displays a Lorentzian-shaped quasiparticle peak near the Fermi energy and a $3d^8$ final-state satellite. In accordance with the Friedel–Anderson model the former is interpreted as due to a single spin-degenerate virtual bound state. The satellite reflects strong electronic correlations in the 3d shell and displays a giant resonance at the Ni 2p edge, allowing an identification of the various d^8 multiplet terms. The effective Coulomb integral U_{eff} of the 3d electrons is estimated from the experimental data, showing a significant reduction from that of Ni-rich alloys. The application of Anderson's criterion for the existence of a local magnetic moment yields the result that the Ni impurities are non-magnetic, in agreement with the Pauli paramagnetism observed in dilute Ni_xAu_{1-x}.

1. Introduction

Transition metals (TM) alloyed into sp metals display interesting electronic and magnetic properties. For example, 3d TM impurities dissolved in noble metals can be either magnetic (e.g. Mn in Au) or non-magnetic (e.g. Ni in Au). It is commonly understood that this behaviour is controlled by an interplay between the interatomic 3d Coulomb interaction and the hybridization of the impurity orbitals with the conduction band states of the host. A theoretical many-body treatment is provided by the Friedel–Anderson model [1–3], which describes a single impurity with localized orbitals placed into a free-electron-gas environment. In the Hartree–Fock solution of the model the impurity states form Lorentzian-shaped 'virtual bound states' (VBS) near the Fermi energy superimposed on the conduction band. Depending on the model parameters the local moment of the TM ion can either be lost upon alloying, with a single VBS equally filled by spin-up and spin-down electrons, or it may survive (though possibly reduced), leading to two VBS split apart at the Fermi level and subsequently unequally populated. Another interesting aspect of TM alloys is the occurrence of correlation effects, which are expected to play an important role in open 3d shells and which go beyond a Hartree–Fock approach. As effective 'zero-3d-bandwidth' materials, dilute alloys with 3d impurities represent excellent model systems for the study of electronic correlations.

A typical example for such systems are the Ni_xAu_{1-x} alloys, which display Pauli paramagnetic behaviour for low Ni concentration ($x < 30\%$) and which are ferromagnetic for $x > 55\%$, with a critical intermediate regime [4, 5]. The Ni impurity states in

† Author to whom any correspondence should be addressed.

0953-8984/96/305569+15$19.50

Au have been studied by various experimental techniques and the results compared to the predictions of the Friedel–Anderson model. Optical absorption [6, 7] and transport measurements [8] could be successfully analysed in terms of a spin-degenerate VBS, but the resulting Lorentzian parameters, obtained in an indirect way, exhibit a considerable scatter (cf. table 1). In contrast, much better access to the impurity states has been obtained by photoelectron spectroscopy [9–12], because it measures the VBS *directly*. The VBS energies thus determined agree reasonably well with the optical data. However, the analysis of the previously reported photoemission data in terms of the Ni 3d density of states is strongly limited by a quite unfavourable Ni 3d/Au 5d photoionization cross section ratio at the photon energies used [9–11]. This results in a relatively low signal-to-noise ratio, leaving uncertainties in the Lorentzian lineshape fits of the VBS peak. The photoemission spectra also yield information about the electronic correlations as indicated by the occurrence of a valence band satellite of $3d^8$ final-state character at higher binding energies. Its multiplet structure has previously been studied in more detail with photon energies around the Ni 3p–3d threshold [12]. Unfortunately, the resonant enhancement of the $3d^8$ final states at this absorption edge is only weak, so only the ^{3}F term could be identified, the others being obscured by the Au 5d emission.

In this work we present synchrotron-radiation-excited photoemission experiments and bremsstrahlung isochromat spectroscopy (BIS) on Ni_xAu_{1-x} alloys in order to study the electronic structure of Ni impurities in Au. Utilizing the Cooper minimum of the Au 5d photoionization cross section and the giant resonance at the Ni 2p–3d absorption edge, the Ni 3d partial density of states becomes strongly enhanced and allows us to perform detailed analyses on the VBS lineshape and the $3d^8$ correlation satellite. The effective Coulomb and exchange integrals of the 3d electrons are estimated from the experiment. Based on the spectroscopically determined energy parameters of the Friedel–Anderson model, we apply Anderson's criterion for the existence of a local magnetic moment to the case of dilute Ni in Au.

2. Sample preparation and experimental details

Ni_xAu_{1-x} alloys with nominal concentrations of $x = 0.05$, 0.10, 0.75, 0.90 and 0.95 were produced by arc melting the pure Ni and Au metals (purity >99.95%) together under an argon atmosphere. They were repeatedly melted to improve the homogeneity, and then cooled rapidly down to room temperature to avoid any segregation. The ellipsoidal specimens obtained in this way were pressed mechanically into pellets and then polished to obtain mirror-like surfaces. During the photoemission measurements the samples were repeatedly cleaned *in situ* (at a base pressure of a few 10^{-10} mbar) with a ceramic scraper to remove surface contaminations. The concentrations obtained from the Ni 2p and Au 4f photoemission intensities agreed with the nominal ones within the experimental accuracy. For Ni-rich samples we observed a slight Au surface enrichment, which was negligible for the Ni-poor samples [13].

Ultraviolet photoelectron spectroscopy (UPS) and BIS studies were performed in our home laboratory with a Vacuum Generators ESCA Mk II spectrometer. The energy resolution was 0.1 eV for He I, 0.2 eV for He II, and 1.0 eV for the BIS spectra, respectively. The synchrotron radiation photoemission studies were carried out using the SX700/II high-performance soft-x-ray monochromator at the synchrotron radiation facility BESSY in Berlin. The photon energy $h\nu$ ranged from 20 to 1000 eV. The total energy resolution, including that of the hemispherical electron energy analyser, was 0.2 eV at $h\nu = 100$ eV and 1.2 eV at $h\nu = 850$ eV. The photon flux was obtained simultaneously by

Table 1. The energy position E_d and the full width at half maximum 2Δ of the virtual bound state in dilute Ni_xAu_{1-x} alloys as obtained in this work and previous studies.

Ni concentration (at.%)	E_d (eV)	2Δ (eV)	Method	Reference
10	$-(0.35 \pm 0.02)$	0.58 ± 0.05	Photoemission (PES)	This work
5	$-(0.41 \pm 0.02)$	0.42 ± 0.04	PES	This work
Dilute limit	$-(0.47 \pm 0.03)$	0.26 ± 0.06	—	This work
10	−0.40	—	PES	[9]
10	−0.40	0.66	PES	[10]
5.0	−0.47	0.50	PES	[11]
4.8	−0.5	—	PES	[12]
2.5	−0.44	0.40	PES	[10]
2	−0.476	0.230	Optical absorption	[6]
2	−0.47	0.216	Optical absorption	[7]
0.62–2.52	−0.26 to −0.24	0.09 to 0.11	Transport	[8]

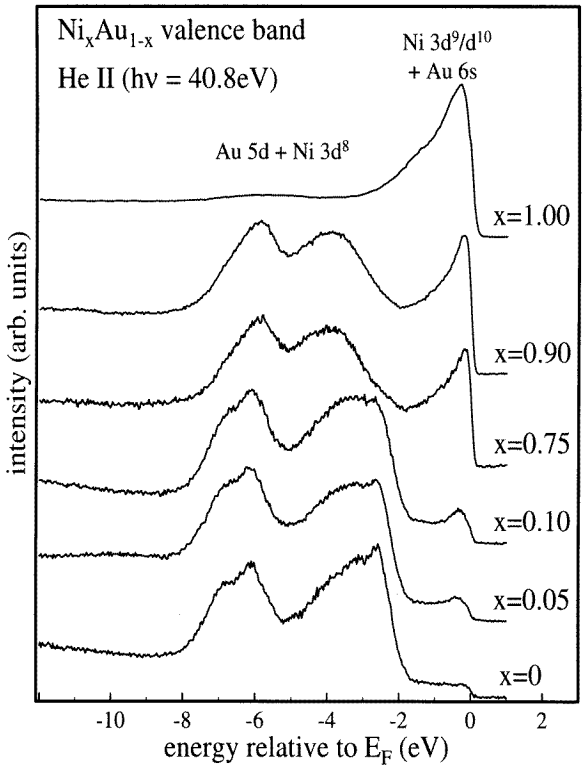

Figure 1. Valence band spectra of various Ni_xAu_{1-x} alloys measured with He II radiation ($h\nu = 40.8$ eV). The spectra are normalized to the same maximum height.

measuring the current of a Au mesh located near the exit slit of the monochromator and used for the normalization of the photoemission and absorption spectra. In order to determine the exact energy position of the Ni 2p absorption threshold for the resonant photoemission

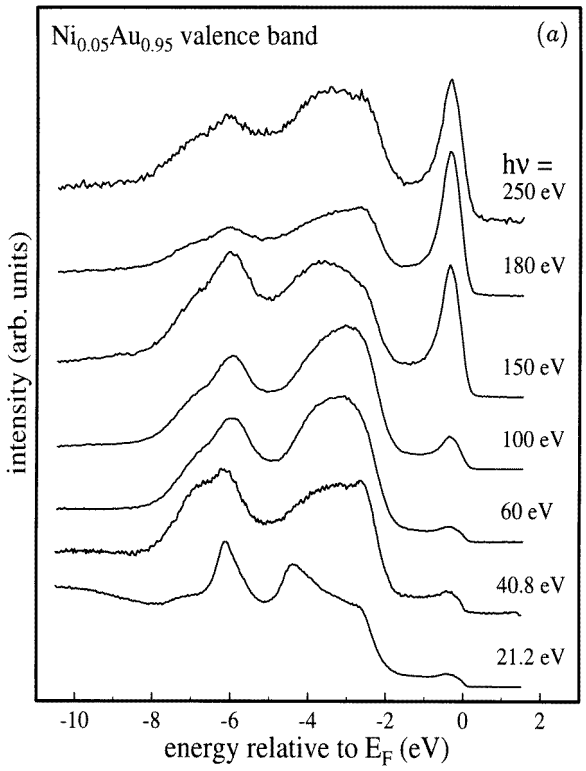

Figure 2. (*a*) Valence band spectra of the dilute alloy $Ni_{0.05}Au_{0.95}$ taken at various photon energies. Spectra are normalized to the same maximum height. Note the enhancement of the VBS peak near E_F relative to the Au 5d emission at $h\nu = 180$ eV. (*b*) Difference spectra obtained from the data in (*a*) and those of pure Au. Also included are the Lorentzian fits of the VBS peak (solid lines).

experiments, the x-ray absorption near-edge structure (XANES) was measured using the total-electron-yield mode.

3. Experimental results and discussions

3.1. Valence band spectra

In figure 1 the valence band spectra of the Ni_xAu_{1-x} alloys with $x = 0$, 0.05, 0.10, 0.75, 0.90 and 1 measured with He II radiation are shown. In agreement with earlier published data [9–12] the alloy valence band can be divided into two spectral ranges: (i) the doublet structure between 2 and 8 eV binding energy, which arises mainly from the spin–orbit-split Au 5d band (with some admixture of Ni $3d^8$-like final states; see discussion further below); and (ii) the Ni 3d states (together with the flat Au 6s and Ni 4s bands) near the Fermi level. For the dilute Ni_xAu_{1-x} alloys the spectra are strongly Au like, with an additional narrow Ni 3d VBS peak on top of the flat Au 6s band. With increasing Ni concentration the VBS is broadened into a Ni metal-like 3d conduction band, while both the Au 5d bandwidth and spin–orbit splitting are decreasing.

In the He II spectra of figure 1 the VBS emission in the Ni-poor alloys is quite weak.

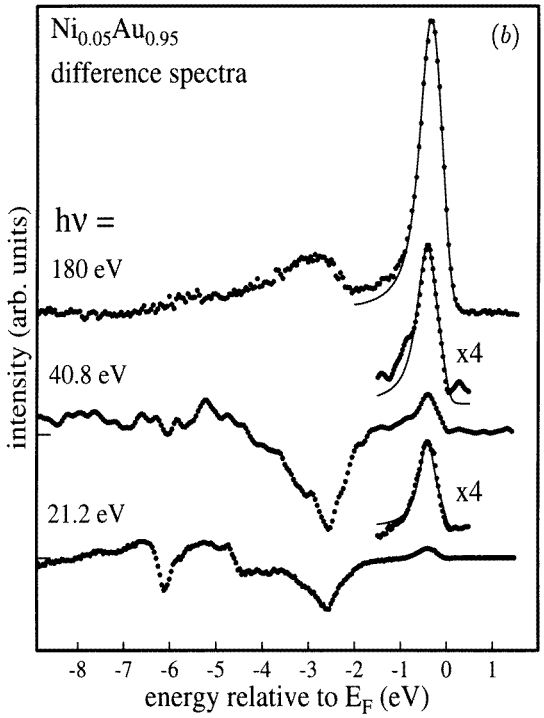

Figure 2. (Continued)

In order to enhance the Ni 3d partial density of states (PDOS) we have utilized the strongly different energy dependence of the Ni 3d and Au 5d photoionization cross sections [12, 14]. Figure 2(*a*) shows valence band spectra of $Ni_{0.05}Au_{0.95}$ taken at various photon energies. Clearly, the Ni 3d/Au 5d intensity ratio increases strongly with photon energy and reaches its maximum at $h\nu = 180$ eV (corresponding to the Au 5d Cooper minimum [14]), where the VBS emission dominates the spectrum. At 180 eV the intensity ratio is enhanced relative to that in the He I and He II spectra by factors of 135 and 88, respectively, in quantitative agreement with the Ni 3d/Au 5d cross section ratio calculated by Yeh and Lindau [14].

In figure 2(*b*) we present difference spectra obtained from some of the spectra in figure 2(*a*) and that of pure Au, which we have used for a further analysis of the Ni 3d PDOS. They were obtained after removing a Shirley-type inelastic background from the corresponding spectra and normalizing them to the Au $5d_{3/2}$ peak at ~ -7 eV, using the assumptions that: (i) there is only a small Ni 3d PDOS at ~ -7 eV; and (ii) the bottom of the Au 5d band is not greatly affected upon alloying. Because the Ni 3d PDOS is strongly enhanced at the Au 5d Cooper minimum, the inaccuracy of this subtraction process (related to the neglect of the Au 5d band narrowing) is negligible at this photon energy. Thus, in contrast to the strongly wiggled structures in the He I and He II difference spectra, a more reliable difference is obtained at $h\nu = 180$ eV, which is similar to that obtained by Folkerts *et al* [12] but with much better energy resolution and data statistics. From these data we find that the Ni 3d impurities form a single VBS-like peak at ~ -0.4 eV and a broad satellite structure within -2 to -6 eV relative to the Fermi level.

In the spirit of the Hartree–Fock approach to the Anderson model [1] we have fitted

the experimental VBS between -1 eV and E_F with a Lorentzian curve, modified with the Fermi–Dirac function at room temperature and convoluted with the Gaussian instrumental response function. Since neither spin–orbit splitting nor crystal-field effects were observed within the experimental accuracy, a single Lorentzian was used [15]. As seen in figure 2(*b*) the fit reproduces the experimental data very well. The binding energy E_d and FWHM 2Δ thus obtained for $Ni_{0.05}Au_{0.95}$ and for $Ni_{0.10}Au_{0.90}$ (not shown here; see [13]) are listed in table 1. The slight energy shift and broadening with Ni concentration reflect the variation of the local chemical environment upon alloying. For example, when going from 5% to 10% concentration the average number of Ni–Ni nearest neighbours increases from 0.6 to 1.2, and the Ni–Ni distance decreases from 2.82 to 2.78 Å [16]. Assuming a linear concentration dependence of both E_d and 2Δ, and extrapolating them to zero concentration, we obtain $E_d \simeq -0.47$ eV and $2\Delta \simeq 0.26$ eV for Ni in the dilute limit. As can be seen in table 1 these results agree well with those obtained by optical spectroscopy [6, 7]. In comparison to previous photoemission studies [9–11] they are more reliable due to the use of a photon energy at the Au 5d Cooper minimum and the resulting strong enhancement of the Ni 3d impurity states.

While the VBS peak is due to quasiparticle excitations, the satellite emission between -2 and -6 eV and the deviation of the high-energy tail of the VBS from the Lorentzian lineshape (cf. figure 2(*b*)) are attributed to correlation effects [12]. They arise from incoherent excitations of the Ni 3d electrons which leave the final $(N-1)$-electron system in a complex many-body state involving more than just one (screened) photohole on a local site. As we will show further below these final states are essentially of Ni $3d^8$ character. It should be noted here that the satellite emission is not reproduced within the Hartree–Fock treatment of the Anderson model, because due to its mean-field character it is an effective one-electron theory which by definition cannot describe correlation effects.

The satellite emission contains for both $Ni_{0.05}Au_{0.95}$ and $Ni_{0.10}Au_{0.90}$ about 24% of the entire (i.e. occupied and unoccupied) Ni 3d spectral weight, where we have modelled the unoccupied part of the VBS by the same Lorentzian as obtained from the above fits of its occupied part. This value agrees well with experimental [17] and theoretically predicted [18] values for pure Ni ($\simeq$20–22%). Furthermore, if we assume this fraction to be valid also in the dilute limit and use the corresponding values for E_d and 2Δ, we find 94% of the entire Ni 3d PDOS to be occupied, resulting in a d occupation n_d of 9.4. This value is in excellent agreement with the one obtained from an analysis of the Ni 2p core-hole satellite ($n_d = 9.33$) [13].

3.2. Bremsstrahlung isochromat spectroscopy (BIS)

The unoccupied density of states has been measured by BIS. Figure 3 shows the spectra measured for alloys with Ni concentrations of $x = 0.05$, 0.10, 0.75, and 0.90 in comparison to those of pure Au and Ni. The Au spectrum displays two broad peaks at $\sim$1.1 and $\sim$3.9 eV, corresponding to the empty Au 6s and 6p states. In contrast, the Ni spectrum shows a relatively narrow peak at $\sim$0.4 eV due to the unoccupied Ni 3d orbitals, superimposed on the broad 4s conduction band. For the Ni_xAu_{1-x} alloys the spectra consist of strongly overlapping partial Au and Ni density of states.

In order to obtain an estimate for the partial Ni 3d spectrum in a dilute alloy we have subtracted the spectra of $Ni_{0.05}Au_{0.95}$ and Au after normalization at 3.0 eV. The difference is displayed in the inset of figure 3 and shows that the unoccupied Ni 3d is centred at about 0.4 eV. For comparison we also show the unoccupied tail of the VBS Lorentzian obtained from the valence band analysis discussed above, convoluted with the Gaussian

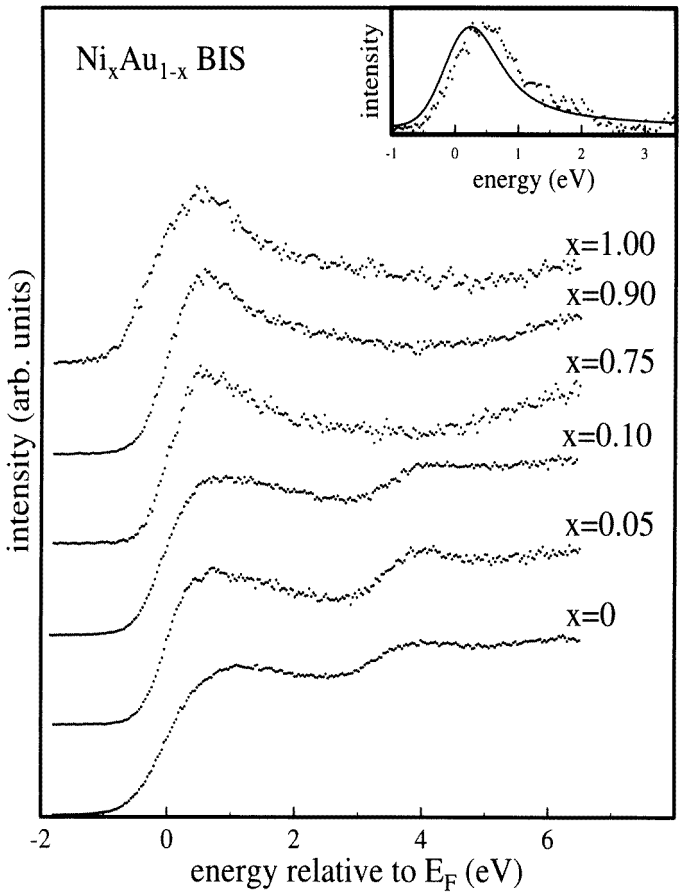

Figure 3. BIS spectra of various Ni_xAu_{1-x} alloys. The inset shows the difference of the $Ni_{0.05}Au_{0.95}$ and Au BIS spectra (points) in comparison to the unoccupied tail of the VBS Lorentzian obtained from the photoemission spectrum (solid line). See the text for details.

instrumental response function of the BIS spectrometer. The resulting curve is shown in the inset as a solid line and reproduces the experimental data quite well. The remaining energy deviation of ∼0.1 eV may be attributed to inaccuracies in the subtraction process and the relatively low resolution of the BIS experiment. This result suggests that the occupied and unoccupied parts of the Ni 3d PDOS near the Fermi level can be described by the same VBS Lorentzian. Neither the photoemission nor the BIS data give any evidence for the existence of two spin-split VBS within the quoted uncertainties of the experiment, thus supporting the view that the dilute Ni impurities form only a single spin-degenerate virtual bound state on top of the broad Au 6s conduction band.

3.3. Resonant photoemission spectroscopy (RPES)

The existence of unoccupied Ni 3d states allows the utilization of resonant photoemission. At the np → 3d absorption threshold ($n = 2, 3$) an interference between the direct photoemission process ($n\mathrm{p}^6\mathrm{3d}^9 + h\nu \rightarrow n\mathrm{p}^6\mathrm{3d}^8\varepsilon_l$) and the core absorption followed by

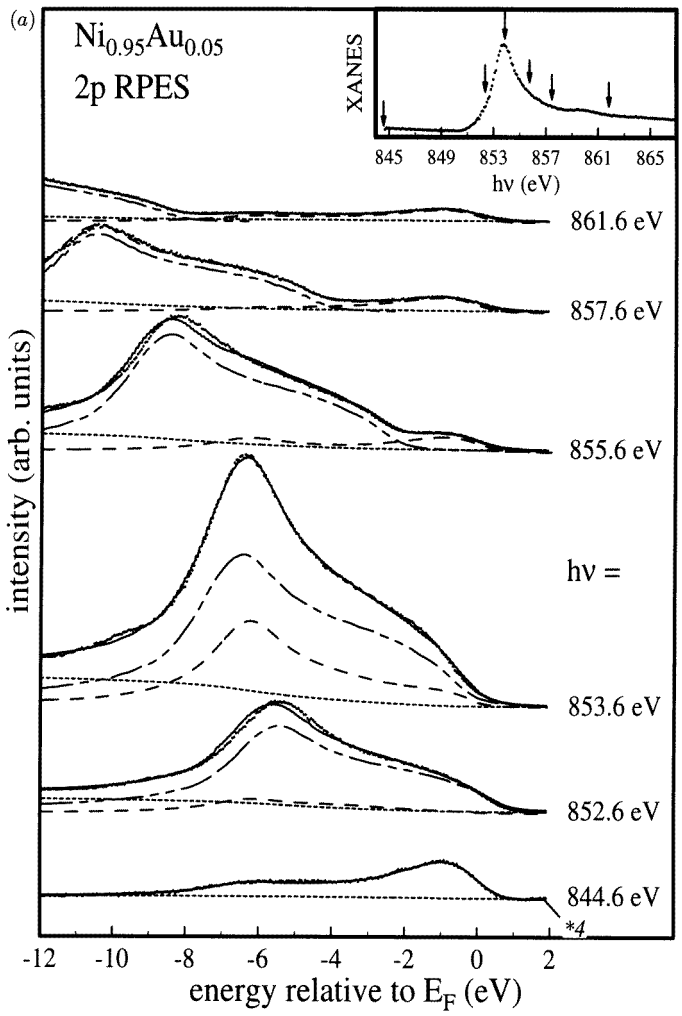

Figure 4. (*a*) $Ni_{0.95}Au_{0.05}$ valence band spectra taken at photon energies near the Ni 2p x-ray absorption threshold (normalized to photon flux) and the model fits for a decomposition of resonant photoemission and incoherent Auger intensities (see the text). Points: experimental data; solid lines through the data: fits; dashed lines: the Ni valence band; dash–dotted lines: the incoherent Auger signal; dotted lines: the inelastic (Shirley-type) background. The corresponding XANES spectrum is shown in the inset. Arrows indicate the photon energies used for the photoemission spectra. (*b*) The corresponding valence band spectrum taken at the Au 5d Cooper minimum (points) and the fit (solid line through the data points). Dashed and dotted lines indicate the 3d quasiparticle band and the $3d^8$ satellite structure, respectively; dash–dotted line: the Shirley background. (*c*) The Ni $L_3M_{4,5}M_{4,5}$ incoherent Auger signal measured with Al Kα radiation (points). Solid line: a fit with four Gaussians; dashed line: the Auger main line (two-hole final states); dash–dotted line: Auger satellites (three- and four-hole final states).

a coherent Auger transition ($np^6 3d^9 + h\nu \rightarrow np^5 3d^{10} \rightarrow np^6 3d^8 \varepsilon_l$) occurs, which enhances the spectral intensity of the $3d^8$ final states. There is still a debate about to what extent *incoherent* Auger emission also contributes to the overall intensity enhancement [19, 20], but as we will show below it is certainly not exclusively due to resonant photoemission.

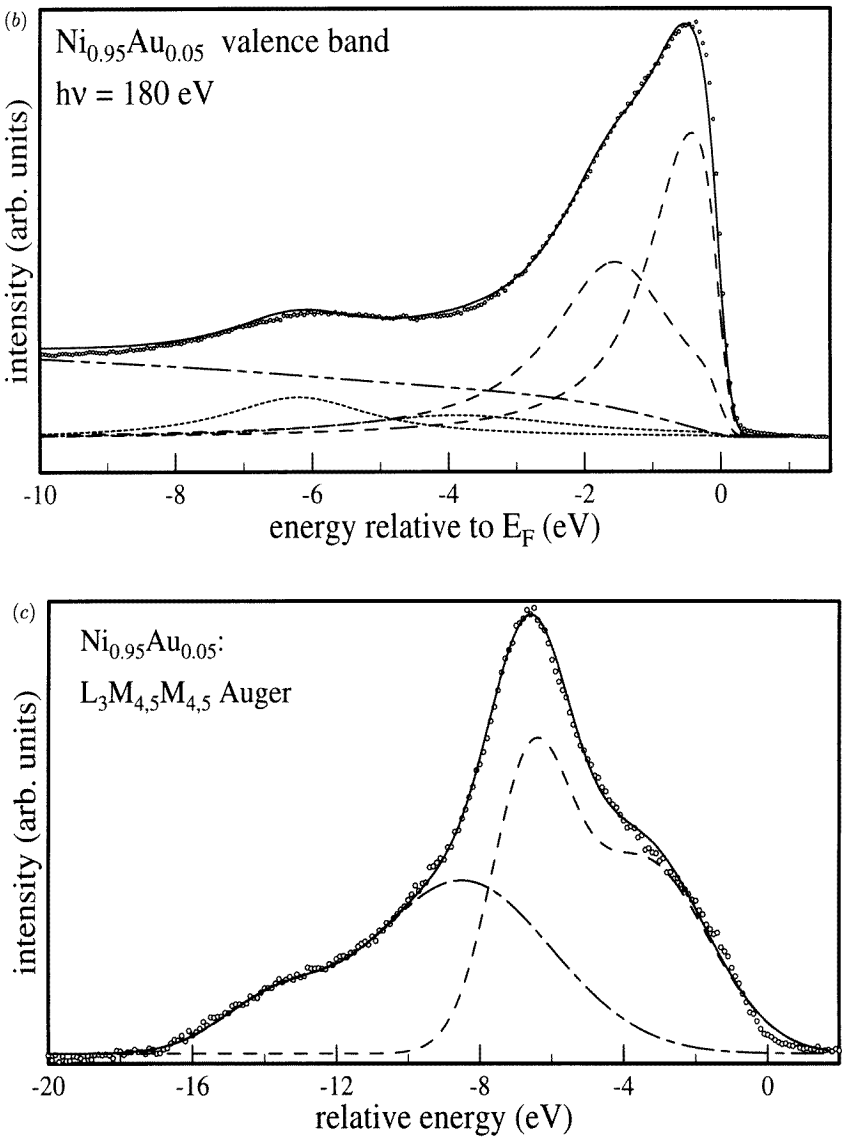

Figure 4. (Continued)

While a previous RPES experiment performed at the 3p–3d edge was limited by the weak resonance and strong Au 5d cross section effects [12], we were able to utilize the much stronger 2p 'giant' resonance for the study of the Ni $3d^8$ satellite. We present here results obtained from both Ni-rich and Ni-poor alloys.

Figure 4(*a*) shows the valence band spectra of $Ni_{0.95}Au_{0.05}$ measured with photon energies around the Ni 2p–3d absorption threshold; the corresponding XANES spectrum is displayed in the inset. At the absorption maximum at 853.6 eV a huge enhancement in the valence band spectrum is observed, with its maximum at about −6 eV relative to the Fermi level. At higher photon energies incoherent Ni $L_3M_{4,5}M_{4,5}$ Auger electrons of

constant kinetic energy are seen to disperse to seemingly higher binding energy. The general resonance behaviour is identical to that in pure Ni [19]. In fact, since the Au concentration is quite low and the Au reference spectra show only a negligible (<1%) intensity variation in this photon energy range, the electronic states of Au do not contribute to this resonance. The observed enhancement arises purely from Ni, namely from a superposition of the resonant $3d^8$ valence band satellite and the incoherent Ni $L_3M_{4,5}M_{4,5}$ Auger signal [19, 20].

Since the relevant physical information of interest here is contained in the $3d^8$ final-state structure, we need to decompose the contributions of satellite emission and incoherent Auger decay. We achieved this by a method employed previously for pure Ni by López *et al* [19], in which the RPES spectra are modelled by a weighted sum of the bare valence band and Auger spectra. For this purpose the valence band was represented by four Lorentzian peaks (multiplied by a Fermi–Dirac function at room temperature and convoluted with the instrumental response function) at −0.4, −1.5, −3.9, and −6.2 eV, as shown in figure 4(*b*). The former two account for the Ni 3d quasiparticle band, while the latter two describe the dominant multiplet terms (^{3}F and ^{1}G) of the $3d^8$ satellite [21]. Similarly, the incoherent Auger spectrum was also represented by four peaks, two accounting for the main line ($3d^8$ final states) and two for the three- ($3d^7$) and four-hole ($3d^6$) satellites [22] (see figure 4(*c*)). The RPES data were then fitted by a linear combination of the Auger spectrum at fixed kinetic energy and the valence band spectrum at the given binding energy, where additionally the relative weights of the respective main lines and satellites were used as free parameters in order to allow for resonance effects. Further details of this procedure are described in [19]. The model spectra thus obtained (also included in figure 4(*a*)) agree well with the measured RPES data. We find that at the absorption maximum, i.e. on resonance, the resonantly enhanced $3d^8$ valence band satellite contributes about 30% to the overall enhancement, with the incoherent Auger signal carrying the major weight. Relative to the Ni 3d quasiparticle band the $3d^8$ emission is enhanced by a factor of ∼17 when compared to the off-resonance spectrum at $h\nu = 844.6$ eV. The satellite is dominated by the ^{1}G term at −6.4 eV, with the centre of gravity of the total $3d^8$ weight lying at −5.4 eV, i.e. at 1 eV lower binding energy.

We further observe that on resonance the incoherent Auger spectrum appears at almost the same energy as the valence band satellite. Their lineshapes are rather similar (except that the Auger signal has more intensity on the high-binding-energy side due to the existence of the d^7 and d^6 final states). For this reason the difference of the on- and off-resonance spectra can be used as an estimate for the spectral distribution of the $3d^8$ photoemission final states, even though at resonance the intensity enhancement is carried predominantly by the incoherent Auger signal and only to a lesser degree by the coherent one. This result is of particular use for the analysis of the RPES data on the dilute alloys presented below, where the low Ni 3d signal makes a full decomposition difficult.

RPES measurements on Ni-poor samples with $x = 0.05$ and 0.10 showed no significant concentration dependence. Therefore we present here only the data obtained for $Ni_{0.10}Au_{0.90}$ because of their better statistics. The corresponding spectra are displayed in figure 5. As is to be expected the valence band emission is strongly Au like. However, in spite of the low Ni concentration a characteristic intensity enhancement centred at ∼−4 eV is observed at the maximum of the Ni 2p–3d absorption ($h\nu = 852.5$ eV). As discussed above, the difference of the on- and off-resonance spectra (presented in figure 6), can be taken as a measure for the $3d^8$ final-state distribution. The $3d^8$ satellite shows a clear multiplet structure caused by the intra-atomic Coulomb interaction. In order to identify the various final-state terms we have calculated the energies of the $3d^8$ terms of a single Ni^{2+} ion, neglecting hybridization between Ni 3d and Au 5d states and using effective Slater integrals $F^{(2)} \simeq 9.6$ eV and

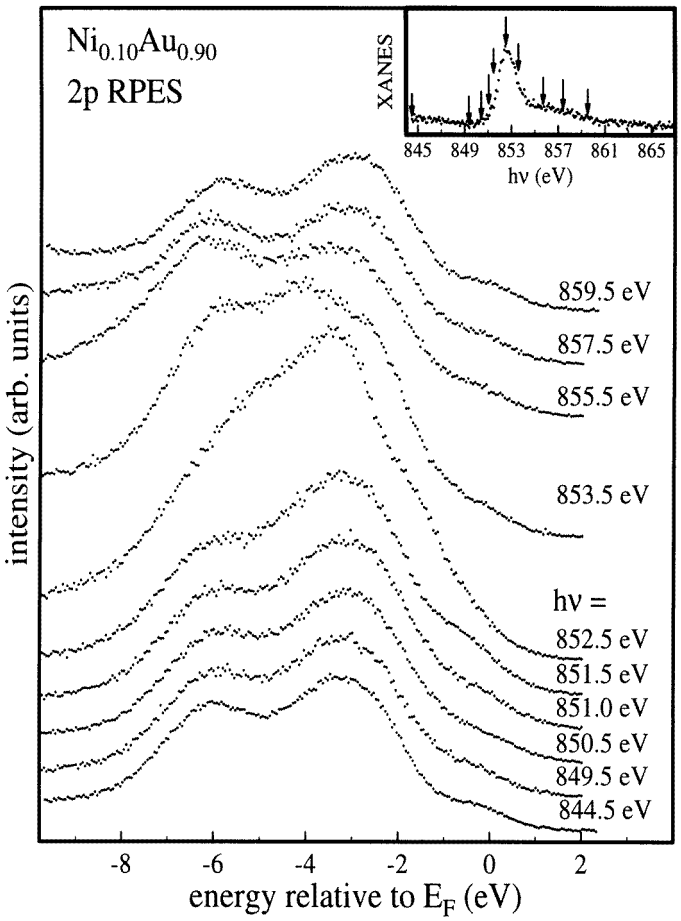

Figure 5. Resonant photoemission spectra of the dilute alloy $Ni_{0.10}Au_{0.90}$ measured near the Ni 2p edge. Inset: the corresponding XANES spectrum.

$F^{(4)} \simeq 6.4$ eV, as obtained in a previous Auger study [21]. The resulting multiplet energies are marked by vertical lines in figure 6, where the ^{1}G term has been fixed at -4.0 eV and the heights of the lines represent the relative intensities. All multiplet terms lie within the enhanced spectral region and agree reasonably well with the experiment, thus confirming our interpretation of the resonant enhancement. In figure 6 we also show for comparison the Ni 3d PDOS as obtained from the valence band spectrum at the Au 5d Cooper minimum. Nice agreement is found between the two spectra in the energy range between -2 and -6 eV, with the ^{1}S term too weak to be distinguished from the background in the Cooper minimum spectrum. The absence of the VBS peak in the resonant spectrum is explained by the fact that due to its d^9/d^{10} character [11, 12] it cannot contribute to the resonance. The structure in the high-binding-energy tail of the VBS can now be attributed to the ^{3}F term of the $3d^8$ multiplet, as concluded from its coincidence with the shoulder in the resonantly enhanced spectrum at -1.8 eV and in agreement with [12]. For the dilute Ni_xAu_{1-x} alloys the overall centre of gravity of the $3d^8$ satellite emission lies at -3 eV, if we assume that it is $\sim$1 eV closer to E_F than the ^{1}G term (as in $Ni_{0.95}Au_{0.05}$).

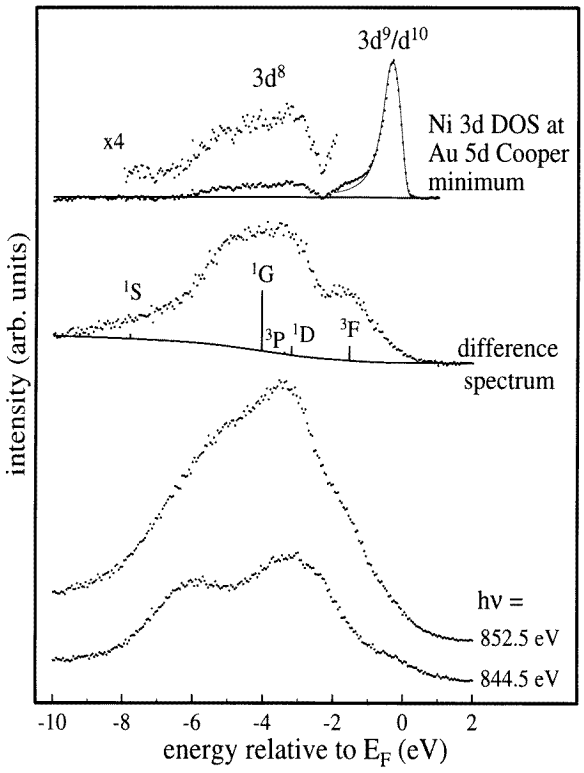

Figure 6. On- and off-resonance spectra from figure 5 and their difference. The vertical lines mark the energies of the various $3d^8$-like final-state terms. The difference of the $Ni_{0.10}Au_{0.90}$ and Au spectra at the Au 5d Cooper minimum is also shown for comparison.

4. Comparison with the Friedel–Anderson model

From the experimental data we can now extract the various parameters of the impurity Hamiltonian describing the dilute Ni_xAu_{1-x} alloys, such as e.g. the effective Coulomb and exchange energies U_{eff} and J_{eff} and the hybridization between the Ni 3d impurity states and the host conduction band. In particular, it becomes possible to verify Anderson's criterion for the existence of a local magnetic moment, $(U_{eff} + 4J_{eff})\rho_d(E_F) > 1$ [1–3], where ρ_d is the impurity DOS per spin and d orbital in the non-magnetic case. We will start with the determination of the effective Coulomb integral.

There are, in principle, two ways to derive U_{eff} from the spectroscopic data. The first one is based on the assumption that in the ground state the Ni impurity is in a local d^9 configuration. In this case the Coulomb energy is reflected in the energy separation between the (centre of gravity of the) $3d^8$ valence band satellite and the $3d^{10}$-like final states of the BIS spectrum, i.e. the unoccupied tail of the VBS. The real ground state of the Ni ion, however, will be a mixture of d^9 and d^{10} states, as implied by the non-integer d occupation obtained in the previous section. As a consequence, the d^8–d^{10} final-state separation will be larger than the actual U_{eff} and thus provide an *upper limit* for the Coulomb energy of the 3d electrons. An alternative approach [11, 12] starts from a d^{10} ground state with only a small d^9 admixture. In this scenario U_{eff} can be determined entirely from the photoemission

valence band spectrum, namely from the binding energy of the $3d^8$ satellite minus twice the quasiparticle energy, i.e. the energy of the VBS peak. With increasing hybridization this value will deviate from the actual U_{eff}, but it is still useful as a *lower limit*. From both methods we thus obtain averaged values for the effective Coulomb integral of 4.4 ± 1.4 eV for Ni-rich alloys and 2.9 ± 0.5 eV for dilute Ni in Au. The former one agrees well with theoretical expectations for pure Ni ($U_{eff} \simeq$ 3–5 eV) [3]. The observed reduction of U_{eff} with decreasing Ni concentration results from a change of the conduction electron density of states at the Fermi level upon alloying, which affects the screening processes [21].

For the determination of the effective exchange energy J_{eff} we utilize the fact that it can be expressed in terms of Slater integrals as $J_{eff} = (F^{(2)} + F^{(4)})/14$ [23]. As shown in the previous section the Ni $3d^8$ final-state multiplet can be well reproduced with $F^{(2)} = 9.6$ eV and $F^{(4)} = 6.4$ eV which yields $J_{eff} \simeq 1.1$ eV for this configuration. According to LDA + U theory [23] the exchange integral is expected to be reduced by about 30% in the ground-state configuration, which is predominantly d^9, resulting in $J_{eff} \simeq 0.8$ eV.

The crucial parameter of the Anderson model is the hybridization integral V_{dk}, which describes the interaction between the localized 3d orbitals and the extended conduction band states and is thus responsible for the charge transfer between the impurity and the host metal. It is related to the half-width of the VBS by $\Delta = \pi \langle |V_{dk}|^2 \rangle \rho_k(E_d)$, where $\rho_k(E_d)$ is the DOS of the conduction band at E_d and $\langle |V_{dk}|^2 \rangle$ is averaged over the energy extension of the VBS [1]. Assuming a flat Au 6s DOS near E_F of $\sim$0.24 eV^{-1}/atom [24] and using Δ for the dilute limit (cf. table 1) yields $\langle |V_{dk}|^2 \rangle = 0.17 \pm 0.04$ eV. It should be possible to obtain a corresponding theoretical estimate for this quantity from *ab initio* calculations of the electronic structure of Ni impurities in a Au host.

The application of the criterion for the existence of local magnetism further requires the knowledge of the partial Ni 3d DOS at the Fermi level. In principle, it can be deduced from the Lorentzian parameters of our VBS fits. However, Anderson's criterion has been derived within the Hartree–Fock approximation [1–3], i.e. neglecting all correlation effects, whereas our photoemission spectra on both the Ni-rich and Ni-poor alloys contain clear evidence for strong electronic correlations. They not only give rise to the intense $3d^8$ two-hole satellite, but will also cause a renormalization of the quasiparticle spectrum. It has been demonstrated [18] by a calculation of the single-particle excitation spectra for pure Ni metal that the inclusion of a suitable self-energy renormalizes the one-electron band energies by a factor of η ($\simeq$0.8) and shifts a fraction $1 - \eta$ of the total spectral 3d weight into the valence band satellite. The fact that the same parameter η describes the quasiparticle renormalization *and* the spectral weight transfer is a direct consequence of the assumption of a local (i.e. k-independent) self-energy. This should be an even better approximation for dilute Ni in a free-electron-like environment. The $3d^8$ weight fraction of 24% determined from our spectra for the Ni-poor alloys implies $\eta \simeq 0.76$. With $E_d = \eta E_d^{HF}$ (where E_d is the measured binding energy of the VBS peak and E_d^{HF} the corresponding (hypothetical) Hartree–Fock energy) we obtain $E_d^{HF} = -0.62$ eV in the dilute limit. Because the hybridization of the 3d impurity states with the conduction band is not expected to be affected much by correlation effects, we can use the Lorentzian half-width of the VBS as measured. From these considerations we obtain an unrenormalized impurity density of states per spin and d orbital of $\rho_d^{HF}(E_F) = 0.10 \pm 0.03$ eV^{-1} within the Hartree–Fock approximation.

Together with the Coulomb and exchange energies derived above, all parameters for Anderson's criterion have now been obtained purely from spectroscopic data. The critical quantity $(U_{eff} + 4J_{eff})\rho_d^{HF}(E_F)$ is found to be 0.6 ± 0.2, much less than unity. Hence, no local magnetic moment should exist for dilute Ni in Au according to the Friedel–Anderson model. This in agreement with the observation that Ni_xAu_{1-x} alloys are Pauli paramagnets

for $x < 30\%$ [4, 5] and confirms our interpretation of the quasiparticle photoemission spectrum as that of a single spin-degenerate virtual bound state.

5. Conclusions

We have investigated the electronic structure of Ni_xAu_{1-x} alloys using photoemission and BIS. The use of synchrotron radiation at the Au 5d Cooper minimum and near the Ni 2p–3d absorption edge allowed us to determine the partial Ni 3d valence band spectra which consist of $3d^9/d^{10}$-like quasiparticle excitations and the $3d^8$ satellite at higher binding energies. For dilute Ni concentrations the former are found to form a single spin-degenerate and Lorentzian-shaped virtual bound state on top of the flat Au 6s conduction band, in accordance with the Friedel–Anderson model. The pronounced two-hole satellite emission indicates strong correlation effects in these alloys and displays a giant resonance at the Ni 2p edge. Care has to be taken to separate the resonant photoemission signal from incoherent Auger intensity. It was possible to identify the various multiplet terms of the d^8 final-state configuration. From combined photoemission and BIS the effective Coulomb integral U_{eff} of the 3d electrons could be derived and found to decrease from Ni-rich to Ni-poor alloys.

From the spectroscopic data we have determined the various parameters of the Anderson Hamiltonian relevant for a Ni impurity in a Au host. In particular, using Anderson's criterion we verified that no local moment exists for dilute Ni, in agreement with the magnetic phase diagram of Ni_xAu_{1-x}. Thus, we conclude that except for the observed correlation effects the Hartree–Fock solution of the Friedel–Anderson model provides a suitable description for the electronic and magnetic properties of the diluted alloys.

Acknowledgments

We wish to thank Professor Inden (Max-Planck-Institut für Eisenhüttenforschung, Düsseldorf) for the Ni_xAu_{1-x} alloys, and the staff of BESSY for their expert help. One of the authors (GM) gratefully acknowledges a grant by the Volkswagen-Stiftung. This work was funded by the BMFT (project 05 5TSAAB3) and the Deutsche Forschungsgemeinschaft.

References

[1] Anderson P W 1961 *Phys. Rev.* **124** 41
[2] Suhl H (ed) 1973 *Magnetism V: Magnetic Properties of Metallic Alloys* (New York: Academic)
[3] Gubanov V A, Liechtenstein A I and Postnikov A V 1992 *Magnetism and the Electronic Structure of Crystals (Springer Series in Solid-State Sciences 98)* (Berlin: Springer)
[4] Kuentzler R and Kappler J P 1979 *J. Phys. F: Met. Phys.* **9** 195
[5] Hurd C M, McAlister S P and Shiozaki I 1981 *Physics of Transition Metals (Inst. Phys. Conf. Ser. 55)* (Bristol: Institute of Physics Publishing) p 475; 1981 *J. Phys. F: Met. Phys.* **11** 457
[6] Bassett M and Beaglehole D 1976 *J. Phys. F: Met. Phys.* **6** 1211
Beaglehole D 1976 *Phys. Rev.* B **14** 341
[7] Lao B Y, Doezema R E and Drew H D 1974 *Solid State Commun.* **15** 1253
[8] Julianus J A, Seewald R, van Nassou N and Bekker F F 1981 *Physics of Transition Metals (Inst. Phys. Conf. Ser. 55)* (Bristol: Institute of Physics Publishing) p 455
[9] Höchst H, Steiner P and Hüfner S 1980 *Z. Phys.* B **38** 201
[10] Reehal H S and Andrews P T 1980 *J. Phys. F: Met. Phys.* **10** 1631
[11] Bosch A, Feil H, Sawatzky G A and Julianus J A 1984 *J. Phys. F: Met. Phys.* **14** 2225
[12] Folkerts W, van der Marel D, Haas C, Sawatzky G A, Norman D, Padmore H, Wright H and Weightman P 1987 *J. Phys. F: Met. Phys.* **17** 657
[13] Knoblauch T 1993 *Diplomarbeit* Universität des Saarlandes

Meng G 1995 *Dissertation* Universität des Saarlandes
[14] Yeh J J and Lindau I 1985 *At. Data Nucl. Data Tables* **32** 1
[15] This is in contrast to the VBS fits in [11], where three Lorentzians were used. Note, however, the extremely low signal-to-noise ratio in that work.
[16] Renaud G, Motta N, Lancon F and Belakhovsky M 1988 *Phys. Rev.* B **38** 5944
[17] Höchst H, Hüfner S and Goldmann A 1977 *Z. Phys.* B **26** 133
[18] Davis L C and Feldkamp L A 1980 *Solid State Commun.* **34** 141
[19] López M F, Höhr A, Laubschat C, Domke M and Kaindl G 1992 *Europhys. Lett.* **20** 357
López M F, Laubschat C and Kaindl G 1993 *Europhys. Lett.* **23** 538
López M F, Laubschat C, Gutiérrez A, Höhr A, Domke M, Kaindl G and Abbate M 1994 *Z. Phys.* B **95** 9
[20] Tjeng L H, Chen C T, Ghijsen J, Rudolf P and Sette F 1991 *Phys. Rev. Lett.* **67** 501
Tjeng L H 1993 *Europhys. Lett.* **23** 535
[21] Bennett P A, Fuggle J C, Hillebrecht F U, Lenselink A and Sawatzky G A 1983 *Phys. Rev.* B **27** 2194
[22] Martensson N, Nyholm R and Johansson B 1984 *Phys. Rev.* B **30** 2245
Sarma D D, Carbone C, Sen P, Cimino R and Gudat W 1989 *Phys. Rev. Lett.* **63** 65
[23] Solovyev I V, Dederichs P H and Anisimov V I 1994 *Phys. Rev.* B **50** 16 861
[24] Weinberger P 1982 *J. Phys. F: Met. Phys.* **12** 2171